URSI GASS 2021, Rome, Italy, 28 August - 4 September 2021

Contact-Free Human Posture Estimation: an Analysis of the Influence of mmWave Array Polarization

Hadi Alidoustaghdam*, André Kokkeler and Yang Miao
Faculty of Electrical Engineering, Mathematics and Computer Science, University of Twente, Enschede, the Netherlands

Abstract

In this paper, the millimeter-wave (mmWave) multiple-input multiple-output (MIMO) array aperture is studied for the capability in estimating human postures in a contact-free manner. A mono-static array with Mills cross topology is utilized for transmitting and receiving the scattered fields from a human body. The 3D image of the human body in the radio "vision" of the array is thus synthesized using the back projection algorithm. In order to conduct a quantitative evaluation of the estimated target geometry associated to postures, the 3D image moments are calculated as the performance metrics. Furthermore, the influence of circular and linear polarization of antenna arrays on generated images are demonstrated. It is shown that linear polarized antennas can capture details of body in simple postures as in standing, however circular polarized antennas can perform satisfactorily in more complex postures as in the sitting. The investigation in this paper is instructive and transferable to specific hardware use cases in practice.

1 Introduction

There is a rapidly growing interest in exploiting mmWave sensing for indoor, outdoor and vehicular environments for assisted-living, assisted-care and assisted-communication [1–3]. Privacy concerns for cameras and limitations of LiDAR in harsh environment direct industry to incorporate radio wave information for sensing [4, 5]. MmWave based contact-free posture estimation serves as a complementary scenario for LiDAR or image based target sensing. Monitoring human posture is a necessity for fall detection and preventive decision making [4]. Human posture estimation by using radio-based technologies has been a research topic for a while [6, 7] and nowadays is proceeded to higher frequencies with allocatable large bandwidth and large antenna elements [4]. With development of mmWave transceivers and array antennas, high resolution sensing became feasible for detecting the details of human body [8]. From the measurable radio propagation channel, the multipath parameters can be estimated and used for constructing an image or forming a point cloud of object. Furthermore, these sparse and incomplete point cloud can be processed for posture classification using machine learning algorithms [4, 5]. Hence the distribution of point cloud is decisive for a successful recognition of posture. The reconstructed image based on the measured scattered field can vary with the polarization of transmit and receive antennas [9]. Since the radar cross section of human body depends on the polarization of incident field [10], we investigate the single person in free space scenario, for the purpose of discovering the influence of source antenna polarization on the posture estimation. In order to study the affect of various polarization on generated point clouds, we chose different antenna polarization for the MIMO topology, then reconstruct the 3D image by Back-projection (BP) algorithm. Quantitative criteria, namely centroid and scaled standard deviation [11] are then considered for the performance assessment of images.

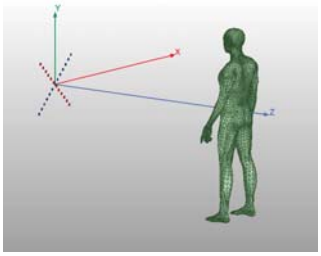

Figure 1. Human standing in front of a MIMO array, red and blue squares are transmitters and receivers, respectively.

2 Formulation

In this section, the algorithm for image reconstruction is introduced. It follows with the definition of a performance metric for evaluating image representativeness for posture estimation.

Let us consider a general scenario in Fig. 1 where a human model is located at a distance of z_o from an antenna aperture with N_T transmitting and N_R receiving antennas. The center of aperture is aligned at the same height with the mass center of body. A distributed target as the human body can be modeled as multiple point scatterers and we consider a single reflection from the point scatterer to the receive antennas. According to BP algorithm [12], a reflectivity image

can be obtained by:

$$I(\boldsymbol{r}) = \int_{k_{\min}}^{k_{\max}} dk \int_{L_{T\min}}^{L_{T\max}} d\boldsymbol{r}_T \int_{L_{R\min}}^{L_{R\max}} d\boldsymbol{r}_R S(\boldsymbol{r}_R, \boldsymbol{r}_T, k) \frac{[\hat{\alpha}_R \cdot \tilde{\boldsymbol{G}}(\boldsymbol{r}_R, \boldsymbol{r}, k)]^*}{|\hat{\alpha}_R \cdot \tilde{\boldsymbol{G}}(\boldsymbol{r}_R, \boldsymbol{r}, k)|^2} \frac{[\hat{\alpha}_T \cdot \tilde{\boldsymbol{G}}(\boldsymbol{r}, \boldsymbol{r}_T, k)]^*}{|\hat{\alpha}_T \cdot \tilde{\boldsymbol{G}}(\boldsymbol{r}, \boldsymbol{r}_T, k)|^2} \quad (1)$$

where $\boldsymbol{r}$ represents position of a point scatterer, $\boldsymbol{r}_T$ and $\boldsymbol{r}_R$ are locations of transmit and receive antennas. $\tilde{\boldsymbol{G}}(\boldsymbol{r}_R, \boldsymbol{r}, k)$ denotes the dyadic Green's function and $k = 2\pi f/c$ is the wave number in free space. $\hat{\alpha}_T$ and $\hat{\alpha}_R$ are the polarization direction of transmit and receive antennas, respectively. The measured scattered field by receive antenna is denoted by S. The * denotes the complex conjugation. $L_{T\max}$, $L_{T\min}$ and $L_{R\max}$, $L_{R\min}$ are the boundaries for locations of transmit and receive antennas, respectively and $k_{\max}$, $k_{\min}$ are the maximum and minimum wavenumbers, respectively. The boundaries of integrals in (1) are determined by desired range and cross-range resolutions [13]. Upon neglecting cross-coupling terms, the dyadic Green's function in the far-field can be approximated by [14]:

$$\tilde{\boldsymbol{G}}(\boldsymbol{r}, \boldsymbol{r}', k) \approx \frac{e^{jk(\boldsymbol{r}-\boldsymbol{r}')}}{|\boldsymbol{r}-\boldsymbol{r}'|} \tilde{\boldsymbol{I}} \quad (2)$$

where $\boldsymbol{r}'$ denotes the location of transmit or receive antenna and $\tilde{\boldsymbol{I}}$ is the identity operator.

Spatial moments are useful tools for preliminary recognition of objects in an image. The spatial moment of order (m,n,p) is defined as [11]:

$$M_{mnp} = \sum_{x,y,z} x^m y^n z^p I_{\text{3-D}}(x,y,z) \quad (3)$$

where the summation is on all the image pixels and $I_{\text{3-D}}(x,y,z)$ is the image intensity. The centeroid of image which is the target location can be calculated as:

$$\tilde{x} = \frac{M_{100}}{M_{000}}, \tilde{y} = \frac{M_{010}}{M_{000}}, \tilde{z} = \frac{M_{001}}{M_{000}} \quad (4)$$

To have an estimation of the size of the target, scaled standard deviation (SSD) [11] can be defined as:

$$\tilde{\sigma}_c = \sqrt{\frac{\sum_{x,y,z}(c-\tilde{c})^2 I_{\text{3-D}}(x,y,z)}{M_{000}}} \quad (5)$$

where c represents the x,y or z and $\tilde{c}$ is the $\tilde{x}$,$\tilde{y}$ or $\tilde{z}$.

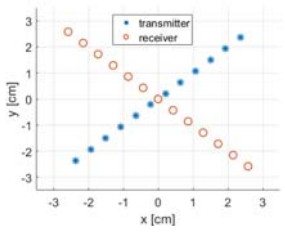

Figure 2. Mills cross array with 12 transmitters and 13 receivers.

3 Numerical Results

The simulation of scattered electric field is implemented in Ansys HFSS based on the shooting and bouncing rays (SBR) technique. Considering $\delta_z = 5$ cm for the range resolution, the frequency of operation is chosen from $f = 33.5$ to 36.5 GHz with 61 samples based on $B = \frac{c}{2\delta_z}$ and $\Delta f = \frac{c}{2D_z}$, in which B is the bandwidth, D_z is the maximum range in investigation domain which is 3 m here and Δf is the frequency sampling step. The resolutions of image in x and y direction δ_x and δ_y referred to as cross-range resolution depend on the aperture size and consequently antenna numbers [13], however sensing of only human posture may not need high cross-range resolution so we consider a limitation of 25 for the antenna numbers. Since the penetration depth of electromagnetic waves in mmWaves is low and in order to reduce the simulation time [15], the human body is modeled as PEC (Perfect Electric Conductor). Human models are created by an open source tool, the Makehuman [16] in standing, lying and sitting postures and located at $z_o = 2$ m distance from the center of antenna aperture as shown in Fig. 3 (a)-(d). The aperture is at the center of coordinate system and directed to the body. To benefit from antennas in a larger aperture and improve the cross-range resolution, conventional Mills cross array [17] as a sparse MIMO topology is chosen where the topology and dimensions are shown in Fig. 2. Each antenna has an idealized beam $\cos^n\theta$ pattern with 45 degree vertical and horizontal beamwidth. Scattered fields are generated by a maximum number of 5 bounces and a ray density of 5 per wavelength. S-parameters of these antennas are recorded and used as the scattered electric fields in (1). As the array is designed by assuming the target in a 2 m distance from the aperture, a domain of $[-1.5,1.5]$m$\times[-1.5,1.5]$m$\times[1,3]$m is divided into pixels with 5 cm length in x, y and z axes then normalized 3D images are obtained. The point clouds are generated and shown in Figs. 3 (e)-(h) for the array with x-polarized antennas. Due to limited aperture of the array, a perfect image of target can not be reconstructed. Depending on the geometry of the target and the incident angle, only a small number of rays is received by aperture and the image is only a representation of points which had a reflection in the receiving domain of the aperture [18]. The centroid and SSDs of human with 4 postures are calculated as in tables 1-4 for different antenna polarization. The RR configuration is defined as transmit and receive antennas being right-hand circularly polarized (RHCP). When the transmit antennas are RHCP whereas receive antennas are left-hand circularly polarized (LHCP), it is referred to as RL configuration [19]. The differences in image centroid and SSD of standing postures and the values for an ideal image are observed here since the perfect images are not reconstructed. The y components of centroids ($\tilde{y}$) have the most variations among the centroid components with posture changes for all polarization configurations. The changes in SSDs are informative as well where the largest SSD component implies the orientation of human body for standing in y-axis or lying in x or z-axis and this is valid for all polariza-

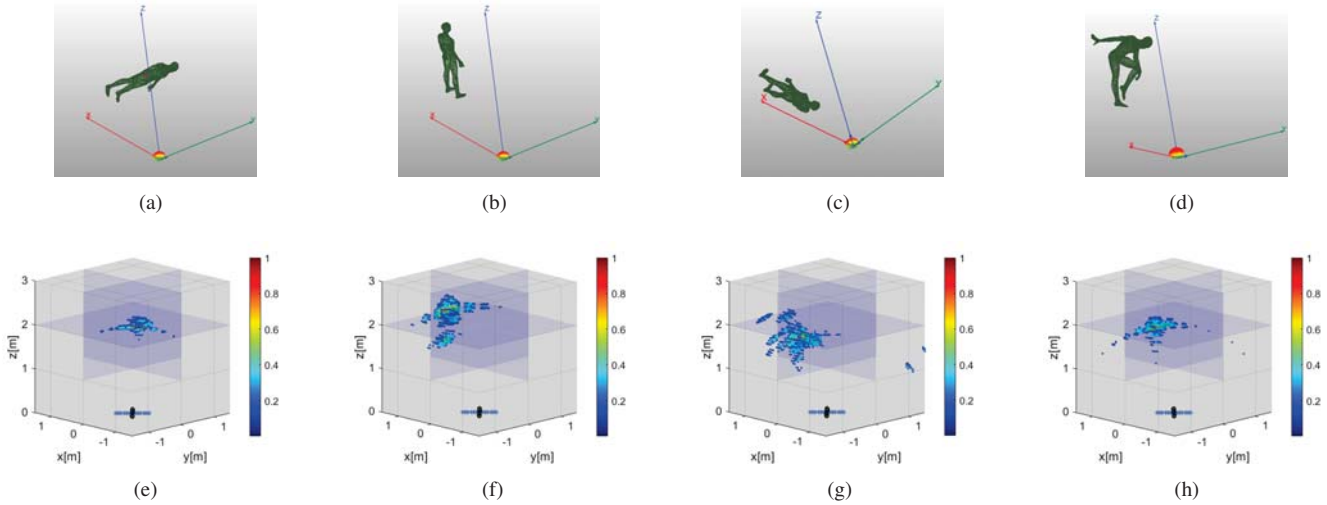

Figure 3. Human with 1.75 m height and 0.5 m shoulder width in (a) standing, (b) lying on z-axis (c) lying on x-axis and (d) sitting posture in front of Mills cross array with x-polarized antennas, the image pixels with intensity more than 0.1 are shown in the point cloud representation for (e) standing, (f) lying on z-axis (g) lying on x-axis and (h) sitting posture. The colors of point clouds indicate reflectivity intensity.

tion configurations as observed in tables 1-4. Considering the geometry of sitting posture, the image should be more distributed and result in almost equal SSD components, where only RR configuration in table. 3 satisfies this criterion whereas other configurations have a concentrated image on the human torso and a small $\tilde{\sigma}_z$ which is not compatible with this sitting posture. Therefore, linear polarized antennas demonstrate enough estimation of simple postures as in standing or lying whereas the RR configuration might provide better information from human body in case of a complex posture as in the sitting. This can be due to the discrimination of fields when scattering from human body

.

Table 1. Array with x-polarized antennas.

Posture	Centroid $(\tilde{x},\tilde{y},\tilde{z})$ [cm]	SSD $(\tilde{\sigma}_x,\tilde{\sigma}_y,\tilde{\sigma}_z)$ [cm]
Standing	(-1.0, 13.8, 194.6)	(14.4, 17.5, 5.4)
Lying in z-axis	(-2.4, -98.4, 243.2)	(18.4, 17.9, 23.6)
Lying in x-axis	(-6.7, -97.3, 188.5)	(35.7, 27.6, 16.5)
Sitting	(0.4, -53.7, 207.1)	(16.9, 20.2, 6.2)

Table 2. Array with y-polarized antennas.

Posture	Centroid $(\tilde{x},\tilde{y},\tilde{z})$ [cm]	SSD $(\tilde{\sigma}_x,\tilde{\sigma}_y,\tilde{\sigma}_z)$ [cm]
Standing	(0.9, 13.0, 195.0)	(14.7, 17.2, 5.7)
Lying in z-axis	(0.7, -97.4, 242.0)	(17.9, 17.6, 30.6)
Lying in x-axis	(-13.4, -100.5, 186.9)	(23.2, 13.5, 8.7)
Sitting	(0.8, -53.7, 207.0)	(16.7, 19.6, 5.9)

Table 3. Array with RR configuration.

Posture	Centroid $(\tilde{x},\tilde{y},\tilde{z})$ [cm]	SSD $(\tilde{\sigma}_x,\tilde{\sigma}_y,\tilde{\sigma}_z)$ [cm]
Standing	(-5.1, 7.5, 203.1)	(28.5, 29.7, 11.4)
Lying in z-axis	(-1.9, -100.0, 237.7)	(17.3, 16.8, 28.4)
Lying in x-axis	(-12.0, -105.6, 194.6)	(23.4, 14.7, 20.5)
Sitting	(1.1, -57.6, 202.5)	(35.1, 36.2, 21.4)

Table 4. Array with RL configuration.

Posture	Centroid $(\tilde{x},\tilde{y},\tilde{z})$ [cm]	SSD $(\tilde{\sigma}_x,\tilde{\sigma}_y,\tilde{\sigma}_z)$ [cm]
Standing	(0.5, 12.7, 193.6)	(14.0, 17.7, 4.6)
Lying in z-axis	(-1.3, -97.3, 245.6)	(12.5, 12.7, 19.4)
Lying in x-axis	(-9.7, -97.9, 187.6)	(31.9, 20.6, 11.8)
Sitting	(1.0, -53.9, 207.1)	(17.0, 19.9, 6.0)

4 Conclusion

In this paper, we proposed a preliminary analysis on a mmWave MIMO array with Mills cross topology for human posture estimation. Linear and circular polarization are chosen and their performances are examined by centroid and standard deviation of generated images. Upon these metrics, it is demonstrated that linear polarized antennas are appropriate for estimation of simple postures however right-hand circular polarization of receive and transmit

antenna attributed better results in a complex posture as in the sitting.

References

[1] S. Z. Gurbuz and M. G. Amin, "Radar-based human-motion recognition with deep learning: Promising applications for indoor monitoring," *IEEE Signal Processing Magazine*, vol. 36, no. 4, pp. 16–28, 2019.

[2] K. Witrisal, P. Meissner, E. Leitinger, Y. Shen, C. Gustafson, F. Tufvesson, K. Haneda, D. Dardari, A. F. Molisch, A. Conti *et al.*, "High-accuracy localization for assisted living: 5g systems will turn multipath channels from foe to friend," *IEEE Signal Processing Magazine*, vol. 33, no. 2, pp. 59–70, 2016.

[3] A. Bourdoux, A. N. Barreto, B. van Liempd, C. de Lima, D. Dardari, D. Belot, E.-S. Lohan, G. Seco-Granados, H. Sarieddeen, H. Wymeersch *et al.*, "6g white paper on localization and sensing," *arXiv preprint arXiv:2006.01779*, 2020.

[4] A. Sengupta, F. Jin, R. Zhang, and S. Cao, "Mm-pose: Real-time human skeletal posture estimation using mmwave radars and cnns," *IEEE Sensors Journal*, vol. 20, no. 17, pp. 10 032–10 044, 2020.

[5] F. Jin, A. Sengupta, and S. Cao, "mmfall: Fall detection using 4-d mmwave radar and a hybrid variational rnn autoencoder," *IEEE Transactions on Automation Science and Engineering*, 2020.

[6] D. Sasakawa, N. Honma, T. Nakayama, and S. Iizuka, "Human posture identification using a mimo array," *Electronics*, vol. 7, no. 3, p. 37, 2018.

[7] M. Zhao, T. Li, M. Abu Alsheikh, Y. Tian, H. Zhao, A. Torralba, and D. Katabi, "Through-wall human pose estimation using radio signals," in *Proceedings of the IEEE Conference on Computer Vision and Pattern Recognition*, 2018, pp. 7356–7365.

[8] B. Gonzalez-Valdes, Y. Álvarez, Y. Rodriguez-Vaqueiro, A. Arboleya-Arboleya, A. García-Pino, C. M. Rappaport, F. Las-Heras, and J. A. Martinez-Lorenzo, "Millimeter wave imaging architecture for on-the-move whole body imaging," *IEEE Transactions on Antennas and Propagation*, vol. 64, no. 6, pp. 2328–2338, 2016.

[9] C. Eyraud, R. Vaillon, A. Litman, J.-M. Geffrin, and O. Merchiers, "Polarization effects in 3d vectorial-induced current reconstructions," *JOSA A*, vol. 30, no. 10, pp. 1967–1974, 2013.

[10] Y. Deep, P. Held, S. S. Ram, D. Steinhauser, A. Gupta, F. Gruson, A. Koch, and A. Roy, "Radar cross-sections of pedestrians at automotive radar frequencies using ray tracing and point scatterer modelling," *IET Radar, Sonar & Navigation*, vol. 14, no. 6, pp. 833–844, 2020.

[11] K. Ren and R. J. Burkholder, "Geometric parameter estimation of buried objects in near-field microwave images," *IEEE Geoscience and Remote Sensing Letters*, 2020.

[12] W. Zhang and A. Hoorfar, "Mimo ground penetrating radar imaging through multilayered subsurface using total variation minimization," *IEEE Transactions on Geoscience and Remote Sensing*, vol. 57, no. 4, pp. 2107–2115, 2018.

[13] J. M. Lopez-Sanchez and J. Fortuny-Guasch, "3-d radar imaging using range migration techniques," *IEEE Transactions on antennas and propagation*, vol. 48, no. 5, pp. 728–737, 2000.

[14] C. Eyraud, J.-M. Geffrin, A. Litman, O. Merchiers, and R. Vaillon, "Effects of polarization on microwave imaging reconstructions," in *2011 International Conference on Electromagnetics in Advanced Applications*. IEEE, 2011, pp. 998–1001.

[15] J. Han, S. Kim, T.-Y. Lee, and M.-H. Ka, "Simplified human model and pedestrian simulation in the millimeter-wave region," in *AIP Conference Proceedings*, vol. 1705, no. 1. AIP Publishing LLC, 2016, p. 020045.

[16] *Make Human*. http://www.makehumancommunity.org.

[17] B. Mills and A. Little, "A high-resolution aerial system of a new type," *Australian Journal of Physics*, vol. 6, no. 3, pp. 272–278, 1953.

[18] S. Y. Seidel and T. S. Rappaport, "Site-specific propagation prediction for wireless in-building personal communication system design," *IEEE transactions on Vehicular Technology*, vol. 43, no. 4, pp. 879–891, 1994.

[19] D. M. Sheen, D. L. McMakin, W. M. Lechelt, and J. W. Griffin, "Circularly polarized millimeter-wave imaging for personnel screening," in *Passive Millimeter-Wave Imaging Technology VIII*, vol. 5789. International Society for Optics and Photonics, 2005, pp. 117–126.